A SIMULATION MODEL FOR SETTLING TANKS WITH VARYING CROSS-SECTIONAL AREA

RAIMUND BÜRGER[A], JULIO CAREAGA[B,*], AND STEFAN DIEHL[C]

Abstract. A quasi–one-dimensional model of the process of continuous sedimentation in vessels with variable cross-sectional area is presented. The partial differential equation (PDE) model extends the settler model advanced in [R. Bürger, S. Diehl, S. Farås, I. Nopens, E. Torfs, Water Sci. Tech. 68 (2013) 192–208], which assumes a constant cross section. A reliable numerical method that handles the special features of the nonlinar PDE is presented along with an advantageous time step condition for continuous and batch sedimentation under the condition of a variable cross-sectional area. Simulations of continuous sedimentation show the effect of the change of cross-sectional area in the concentration inside the vessel and in the underflow. Simulations of batch settling in cones illustrate the versatility of the numerical scheme to include a vertex, where the area shrinks to zero.

Keywords: continuous sedimentation, secondary clarifier, simulation model, wastewater treatment, water resource recovery facilities

Nomenclature

A	cross-sectional area [m^2]
B	depth of thickening zone [m]
C	concentration inside SST [kg/m^3]
$\hat{C}$	maximum point of f_{bk} [kg/m^3]
C_{c}	critical concentration [kg/m^3]
C_j	concentration in layer j (7) [kg/m^3]
$C_{\max}$	maximum concentration [kg/m^3]
D	primitive of d_{comp} (11) [kg/(ms)]
$\mathcal{F}$	(convective) flux function [kg/s]
G_j	Godunov numerical flux (8) and (9) [kg/(m^{2}s)]
H	height of clarification zone [m]
J_{comp}	compressive flux (12) [kg/(m^{2}s)]
J_{disp}	dispersive flux (13) [kg/(m^{2}s)]
N	number of layers inside SST [−]
Q	volumetric flow rate [m^3/s]
T	total simulation time [s]

Date: April 6, 2017.

*Corresponding author.

[A]CI^{2}MA and Departamento de Ingeniería Matemática, Facultad de Ciencias Físicas y Matemáticas, Universidad de Concepción, Casilla 160-C, Concepción, Chile. E-Mail: rburger@ing-mat.udec.cl.

[B]CI^{2}MA and Departamento de Ingeniería Matemática, Facultad de Ciencias Físicas y Matemáticas, Universidad de Concepción, Casilla 160-C, Concepción, Chile. E-Mail: juliocareaga@udec.cl.

[C]Centre for Mathematical Sciences, Lund University, P.O. Box 118, S-221 00 Lund, Sweden. E-Mail: diehl@maths.lth.se.

d_{comp} compression function (5) [m^2/s]
d_{disp} dispersion function (6) [m^2/s]
f_{bk} Kynch batch flux density function [$\mathrm{kg}/(\mathrm{m}^2\mathrm{s})$]
g acceleration of gravity [m/s^2]
j layer index [$-$]
q parameter in settling velocity function (20) [$-$]
t time [s]
v_0 settling velocity of a single particle in unbounded fluid [m/s] (20)
v_{hs} hindered settling velocity [m/s]
z depth from feed level in SST [m]

Greek letters

Δt time step of numerical method [s]
Δz layer width of numerical method [m]
Ψ (total) flux (2) [kg/s]
α parameter in effective solid stress function (21) [$\mathrm{m}^2/\mathrm{s}^2$]
α_1 parameter in dispersion coefficient (22) [m^{-1}]
α_2 parameter in dispersion coefficient (22) [s/m^2]
γ characteristic function (4), equals 1 inside and 0 outside SST
δ Dirac delta distribution [m^{-1}]
ρ_{f} density of fluid [kg/m^3]
ρ_{s} density of solids [kg/m^3]
σ_{e} effective solid stress (21) [Pa]

Introduction

Benchmark simulations of water resource recovery facilities (wastewater treatment plants) are often made with one-dimensional (1D) simulation models of the secondary settling tank (SST) to avoid the computational complexity of higher-dimensional models. It is usually assumed that the cross-sectional area is the same at all depths. The bottom of an SST is, however, often sloped and the space occupied by the feed inlet in circular SSTs clearly shows that the cross-sectional area varies with depth. Furthermore, batch settling experiments are sometimes made in conical vessels. Instead of taking the larger step to model settling in 2D or 3D (Samstag et al., 2016), we include a varying cross-sectional area into a 1D model. A reliable numerical method is obtained by the consistent modelling methodology (Bürger et al., 2011), starting from the integral form of the conservation law.

The aim of this work is to extend the 1D simulation model of SSTs, presented in (Bürger et al., 2011, 2013) and evaluated in (Bürger et al., 2012a; Torfs et al., 2015), to include the case of a varying cross-sectional area $A(z)$; see Figure 1. The model can be written as the following partial differential equation (PDE):

$$\frac{\partial \left(A(z)\, C\right)}{\partial t} + \frac{\partial}{\partial z}\mathcal{F}(C,z,t) = \frac{\partial}{\partial z}\left(A(z)\big\{\gamma(z) d_{\mathrm{comp}}(C) + d_{\mathrm{disp}}(z,Q_{\mathrm{f}}(t))\big\}\frac{\partial C}{\partial z}\right) + Q_{\mathrm{f}}(t) C_{\mathrm{f}}(t)\delta(z),$$

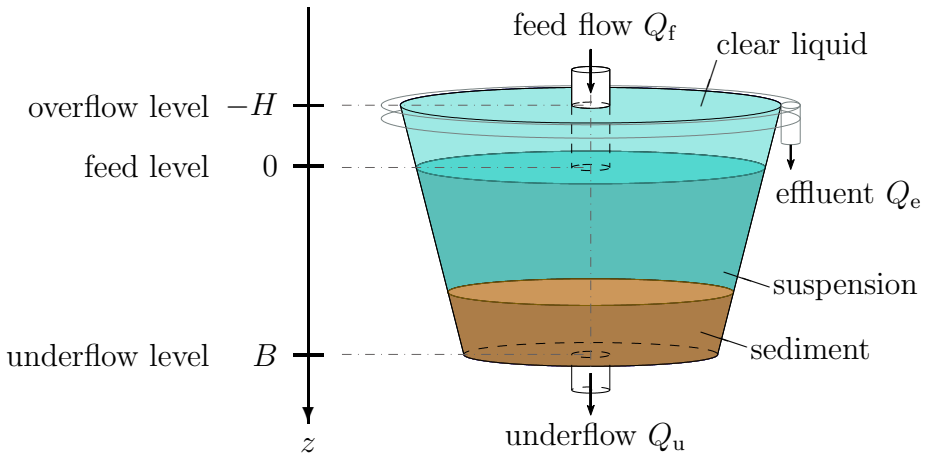

FIGURE 1. Schematic illustration of an SST. The suspension of activated sludge of concentration $C_\mathrm{f}(t)$ streams into the SST at the feed level $z = 0$ at the volumetric flow $Q_\mathrm{f}(t) \geq 0$. The volumetric flows out of the SST are $Q_\mathrm{u}(t) \geq 0$ at the underflow level $z = B$ and $Q_\mathrm{e}(t) := Q_\mathrm{f}(t) - Q_\mathrm{u}(t) \geq 0$ at the effluent level $z = -H$. It is assumed that C_f, Q_f and Q_u are given functions of t.

where $C := C(z,t)$ is the unknown solids concentration function of depth z and time t, $\mathcal{F}$ is a flux function that models the volumetric bulk flows and hindered settling and contains $A(z)$, d_comp models compression of the particles at high concentrations, and d_disp describes dispersion near the feed inlet. The feed mechanism is modelled by the last term.

Continuous sedimentation in vessels with variable area are used for activated sludge (De Clercq et al., 2003; Stepova and Kalugin, 2011; Watts et al., 1996) and other materials (Jiao et al., 2013; Silva et al., 2003; White and Verdone, 2000). In comparison to the few previous works on 1D models with both varying area and compression; e.g. (Bürger et al., 2004, 2005), the novelties are (i) a new and improved CFL condition (time step size stability condition), which implies faster simulations, (ii) a numerical method described explicitly for implementation, and (iii) the possibility of simulating also sedimentation in a cone, for which the cross-sectional area tends to zero at the bottom.

The study of settling in cones is partially motivated by the widespread use of so-called Imhoff cones in wastewater treatment (Folens et al., 2016; van der Steen et al., 2015; Park and Craggs, 2014). Moreover, the advantage of using a cone instead of a cylinder for identifying the hindered settling flux function based on solutions of the model PDE was recently elaborated in (Bürger et al., 2017). We therefore include a section on the implementation of the method for batch sedimentation, which can be used for vessels having constant or varying cross section.

MATHEMATICAL MODEL

Figure 1 shows a schematic view of an axisymmetric SST. The vessel corresponds to the depth interval $-H \leq z \leq B$ and the regions $z < -H$ and $z > B$ are included for mathematical reasons; however, parts of them can be seen as the outlet pipes. In this way,

the problem can be formulated on the entire vertical axis, which means that no boundary conditions need to be imposed.

Let us consider an arbitrary interval (z_1, z_2) of the depth axis. The conservation law of mass states that the rate of increase of mass in (z_1, z_2) equals the signed flux in $\Psi|_{z=z_1}$ minus the flux out $\Psi|_{z=z_2}$ plus the source contribution inside the interval:

$$\frac{\mathrm{d}}{\mathrm{d}t}\int_{z_1}^{z_2} A(z)C(z,t)\,\mathrm{d}z = \Psi|_{z=z_1} - \Psi|_{z=z_2} + \int_{z_1}^{z_2} Q_{\mathrm{f}}(t)C_{\mathrm{f}}(t)\delta(z)\,\mathrm{d}z, \tag{1}$$

where Ψ denotes the total flux given by

$$\Psi\left(C, \frac{\partial C}{\partial z}, z, t\right) = \mathcal{F}(C,z,t) - A(z)\big\{\gamma(z)d_{\mathrm{comp}}(C) + d_{\mathrm{disp}}(z, Q_{\mathrm{f}}(t))\big\}\frac{\partial C}{\partial z}. \tag{2}$$

The conservation law (1) can be also formally written as the PDE

$$\begin{aligned} &\frac{\partial\left(A(z)\,C\right)}{\partial t} + \frac{\partial}{\partial z}\left(\mathcal{F}(C,z,t)\right) = \\ &\frac{\partial}{\partial z}\left(A(z)\big\{\gamma(z)d_{\mathrm{comp}}(C) + d_{\mathrm{disp}}(z, Q_{\mathrm{f}}(t))\big\}\frac{\partial C}{\partial z}\right) + Q_{\mathrm{f}}(t)C_{\mathrm{f}}(t)\delta(z). \end{aligned} \tag{3}$$

A numerical method is derived, however, from the integral form (1). The convective flux function $\mathcal{F}$ (mass per time unit) involves the hindered settling flux function $f_{\mathrm{bk}}(C) = Cv_{\mathrm{hs}}(C)$, where v_{hs} is the hindered settling velocity function, which satisfies $v_{\mathrm{hs}}(C_{\max}) = 0$. We need to define a maximum concentration $C_{\max}$ for the numerical method (for the CFL condition). The flux $\mathcal{F}$ also includes the volumetric flows $Q_{\mathrm{e}}(t)$, $Q_{\mathrm{u}}(t)$ and the area $A(z)$:

$$\mathcal{F}(C,z,t) := \begin{cases} -Q_{\mathrm{e}}(t)C & \text{if } z < -H, \\ -Q_{\mathrm{e}}(t)C + A(z)f_{\mathrm{bk}}(C) & \text{if } -H \le z < 0, \\ Q_{\mathrm{u}}(t)C + A(z)f_{\mathrm{bk}}(C) & \text{if } 0 < z \le B, \\ Q_{\mathrm{u}}(t)C & \text{if } z > B. \end{cases}$$

This means that in the effluent ($z < -H$) and underflow ($z > B$) regions, the sludge is assumed to follow the bulk streams. Consequently, compression and dispersion are assumed to occur only inside the vessel and $\gamma = \gamma(z)$ indicates whether z is a depth in the interior or the exterior of the SST, i.e.,

$$\gamma(z) := \begin{cases} 1 & \text{for } -H \le z \le B, \\ 0 & \text{for } z < -H \text{ or } z > B. \end{cases} \tag{4}$$

The compression function

$$d_{\mathrm{comp}}(C) = \frac{\rho_{\mathrm{s}}}{\rho_{\mathrm{s}} - \rho_{\mathrm{f}}} v_{\mathrm{hs}}(C)\sigma_{\mathrm{e}}'(C) \tag{5}$$

contains the densities of the solids (ρ_{s}) and the fluid (ρ_{f}), the hindered settling velocity v_{hs} and the derivative of the effective solid stress function $\sigma_{\mathrm{e}}'(C)$, which satisfies

$$\sigma_{\mathrm{e}}'(C)\begin{cases} = 0 & \text{for } C < C_{\mathrm{c}}, \\ > 0 & \text{for } C \ge C_{\mathrm{c}}, \end{cases}$$

where C_c is the critical concentration above which compression occurs. With the dispersion function $d_\mathrm{disp}(z, Q_\mathrm{f})$ one can model mixing phenomena caused by the inlet stream at $z = 0$. Naturally, such are assumed to occur only inside the SST; hence, we assume that

$$d_\mathrm{disp}\big(z, Q_\mathrm{f}(t)\big) \begin{cases} = 0 & \text{for } z \le -H \text{ and } z \ge B, \\ \ge 0 & \text{for } -H < z < B. \end{cases} \tag{6}$$

The last term of (1) or (3), which contains the delta Dirac distribution $\delta(z)$, models the mass per time unit fed into the SST from the biological reactors.

The model is closed when the two constitutive functions, hindered settling velocity $v_\mathrm{hs}(C)$ and effective solid stress $\sigma_\mathrm{e}(C)$, and the empirical dispersion function $d_\mathrm{disp}(z, Q_\mathrm{f})$ have been specified.

As mentioned, no boundary condition is needed in this problem. Initial data inside the SST,

$$C(z, 0) = C_0(z), \quad -H \le z \le B,$$

is sufficient for a well-defined problem, since the effluent and underflow concentrations are naturally defined for $t > 0$ because of the direction of the outlet flows (assuming these are nonzero). In the outlet pipes, the area function can for simplicity be defined as $A(z) = A(-H)$ for $z \le -H$ and $A(z) = A(B)$ for $z > B$. The actual size of an outlet pipe will only influence dynamic transients of the underflow concentration $C_\mathrm{u}(t)$ but not stationary solutions (this is explained in connection to (15)).

Numerical scheme

The numerical method is derived from the integral version of the conservation law (1) as was done by Bürger et al. (2013); however, now with care taken for the z-dependence of the cross-sectional area $A(z)$.

Spatial discretization. The spatial domain $[-H, B]$ is divided into N computational cells, or layers, each of the width $\Delta z = (H + B)/N$, separated by $z_j := j\Delta z - H$ for $j = 0, \ldots, N$ where $z_0 = -H$ and $z_N = B$ are the top and bottom of the vessel; cf. Bürger et al. (2013, Figure 2). The j-th layer corresponds to the interval $[z_{j-1}, z_j]$ with centre $z_{j-1/2} := (j - 1/2)\Delta z - H$. We suppose that the feed mechanism is located inside the feed layer $(z_{j_\mathrm{f}-1}, z_{j_\mathrm{f}}]$, where $j = j_\mathrm{f} := \lceil H/\Delta z \rceil$ is the nearest integer larger than or equal to $H/\Delta z$. For the correct approximation of the second-order derivatives it is necessary to introduce one extra layer in the effluent and underflow zone, respectively. As in (Bürger et al., 2013), we add still another one in each zone in order to show how the update formulas look like in case one wishes to model a certain outlet pipe length.

We define $C_j = C_j(t)$ as the average of the exact solution C over layer j at time t:

$$C_j(t) := \frac{1}{\Delta z} \int_{z_{j-1}}^{z_j} C(z, t)\, \mathrm{d}z. \tag{7}$$

Then the left-hand side of (1), with the integral taken over layer j, can be approximated as follows, where $A_{j-1/2} := A(z_{j-1/2})$:

$$\frac{\mathrm{d}}{\mathrm{d}t} \int_{z_{j-1}}^{z_j} A(z) C(z, t)\, \mathrm{d}z \approx A(z_{j-1/2}) \frac{\mathrm{d}}{\mathrm{d}t} \int_{z_{j-1}}^{z_j} C(z, t)\, \mathrm{d}z = A_{j-1/2} \Delta z \frac{\mathrm{d}C_j}{\mathrm{d}t}.$$

The fluxes between layers are approximated consistently with the right-hand side of (1). For the flux $\mathcal{F}$, we use an upwind scheme for the bulk velocities and the Godunov flux for the settling flux in the following way. At $z = z_j$ between layers j and $j+1$, we define

$$\mathcal{F}_j^{\mathrm{num}} := \begin{cases} -Q_{\mathrm{e}}(t)C_{j+1} & \text{if } j = -1, \\ -Q_{\mathrm{e}}(t)C_{j+1} + A(z_j)G_j & \text{if } j = 0, \ldots, j_{\mathrm{f}} - 1, \\ Q_{\mathrm{u}}(t)C_j + A(z_j)G_j & \text{if } j = j_{\mathrm{f}}, \ldots, N, \\ Q_{\mathrm{u}}(t)C_j & \text{if } j = N+1, \end{cases} \tag{8}$$

where the Godunov numerical flux is

$$G_j := \begin{cases} \min\limits_{C_j \le C \le C_{j+1}} f_{\mathrm{bk}}(C) & \text{if } C_j \le C_{j+1}, \\ \max\limits_{C_j \ge C \ge C_{j+1}} f_{\mathrm{bk}}(C) & \text{if } C_j > C_{j+1}. \end{cases} \tag{9}$$

For a unimodal function f_{bk} with maximum point $\hat{C}$, the flux G_j can be computed by Algorithm 1 of (Bürger et al., 2013) or the following compact formula (Adimurthi et al., 2004):

$$G_j = \min\left\{f_{\mathrm{bk}}(\min\{C_j, \hat{C}\}), f_{\mathrm{bk}}(\max\{C_{j+1}, \hat{C}\})\right\}. \tag{10}$$

To obtain a stable numerical method, we define the primitive of the compression function $d_{\mathrm{comp}}(C)$, which is zero for $C < C_{\mathrm{c}}$,

$$D(C) := \int_{C_{\mathrm{c}}}^{C} d_{\mathrm{comp}}(s)\,\mathrm{d}s, \tag{11}$$

and the compressive and dispersive fluxes as

$$J_{\mathrm{comp}}(z,t) := \gamma(z) d_{\mathrm{comp}}(C)\frac{\partial C}{\partial z} = \gamma(z)\frac{\partial D(C)}{\partial z}, \tag{12}$$

$$J_{\mathrm{disp}}(z,t) := d_{\mathrm{disp}}(z, Q_{\mathrm{f}}(t))\frac{\partial C}{\partial z}. \tag{13}$$

These two fluxes are approximated by

$$J_{\mathrm{comp},j}^{\mathrm{num}} := \gamma(z_j)\,\frac{D_{j+1}^{\mathrm{num}} - D_j^{\mathrm{num}}}{\Delta z} \quad \text{and} \quad J_{\mathrm{disp},j}^{\mathrm{num}} := d_{\mathrm{disp},j}\,\frac{C_{j+1} - C_j}{\Delta z},$$

where $d_{\mathrm{disp},j} := d_{\mathrm{disp}}(z_j, Q_{\mathrm{f}}(t))$, and $D_j^{\mathrm{num}} := D(C_j)$. If the primitive $D(C)$ is not available in closed algebraic form, then D_j^{num} has to be computed numerically; see (Bürger et al., 2013, Algorithms 3.2–3.3).

The conservation law for layer j (cf. (1)) can be written in the method-of-lines (MOL) form

$$\begin{aligned} \frac{\mathrm{d}C_j}{\mathrm{d}t} = &- \frac{\mathcal{F}_j^{\mathrm{num}} - \mathcal{F}_{j-1}^{\mathrm{num}}}{A_{j-1/2}\Delta z} + \frac{A_j J_{\mathrm{comp},j}^{\mathrm{num}} - A_{j-1} J_{\mathrm{comp},j-1}^{\mathrm{num}}}{A_{j-1/2}\Delta z} \\ &+ \frac{A_j J_{\mathrm{disp},j}^{\mathrm{num}} - A_{j-1} J_{\mathrm{disp},j-1}^{\mathrm{num}}}{A_{j-1/2}\Delta z} + \frac{Q_{\mathrm{f}}(t)C_{\mathrm{f}}(t)}{A_{j-1/2}\Delta z}\delta_{j,j_{\mathrm{f}}}, \quad j = -1, \ldots, N+2, \end{aligned} \tag{14}$$

where $\delta_{j,j_{\mathrm{f}}} = 1$ if $j = j_{\mathrm{f}}$ and $\delta_{j,j_{\mathrm{f}}} = 0$ otherwise. For example, we get for the first layer below the underflow level (in the underflow pipe)

$$\frac{\mathrm{d}C_{N+1}}{\mathrm{d}t} = -\frac{Q_{\mathrm{u}}}{A_{N+1/2}\Delta z}(C_{N+1} - C_N) + \frac{A_N G_N}{A_{N+1/2}\Delta z} - \frac{A_N\left(D_{N+1}^{\mathrm{num}} - D_N^{\mathrm{num}}\right)}{A_{N+1/2}(\Delta z)^2}, \tag{15}$$

In steady state when time derivatives are zero, (15) implies that C_{N+1} is independent of $A_{N+1/2}$, i.e., the area of the outlet pipe does not influence the underflow concentration.

Time discretization. The MOL equations (14) can in principle be solved by any standard ODE solver. This is convenient when these SST equations are solved together with ODEs modelling biological reactions in the activated sludge process. Implicit-type ODE solvers have the advantage that no upper limit of the time-step size needs to be substituted by the user, but other disadvantages: they may be slow or even fail when the right-hand sides contain functions that are not continuously differentiable, like the Godunov flux (8). Explicit ODE solvers are easiest to implement, but require an upper limit for the time step (CFL condition). Considering the errors created by the spatial discretization, there is no point in using any more advanced solver than the simple finite difference step (Diehl et al., 2015):

$$\frac{\mathrm{d}C_j}{\mathrm{d}t} \approx \frac{C_j^{n+1} - C_j^n}{\Delta t}, \tag{16}$$

where $C_j^n := C_j(t_n) \approx C(z_j, t_n)$ is the approximate concentration at the discrete time points $t_n = n\Delta t$, $n = 0, 1, 2, \ldots$. With (16) inserted into (14), and the right-hand side evaluated at time t_n, the explicit numerical method can be written as follows, where the index n means evaluation of a time-dependent function at $t = t_n$,

$$\begin{aligned} C_j^{n+1} = C_j^n - \frac{\Delta t}{A_{j-1/2}\Delta z}\Big(& \mathcal{F}_j^{\mathrm{num},n} - \mathcal{F}_{j-1}^{\mathrm{num},n} - A_j J_{\mathrm{comp},j}^{\mathrm{num},n} + A_{j-1} J_{\mathrm{comp},j-1}^{\mathrm{num},n} \\ & - A_j J_{\mathrm{disp},j}^{\mathrm{num},n} + A_{j-1} J_{\mathrm{disp},j-1}^{\mathrm{num},n} - Q_{\mathrm{f}}^n C_{\mathrm{f}}^n \delta_{j,j_{\mathrm{f}}} \Big), \\ & j = -1, \ldots, N+2, \quad n = 0, 1, 2, \ldots . \end{aligned} \tag{17}$$

CFL condition. The nonlinearities of the flux function f_{bk} (or G_j) and the spatial derivatives in the PDE (3) imply that instabilities and non-physical solutions can occur if the time step Δt is too large in comparison to the chosen spatial resolution Δz. Fortunately, an upper bound for Δt can be computed beforehand and such is called a CFL condition. More information and examples on the importance of the CFL condition and variants of it for different time-stepping methods are provided by Bürger et al. (2005, 2013); Diehl et al. (2015). In the case of a varying cross-sectional area $A(z)$, the CFL condition becomes even more restrictive. Previous published numerical methods for continuous sedimentation in a vessel with varying cross-sectional area (Bürger et al., 2004, 2005) have focussed on proving convergence of the numerical solution to the exact one of the PDE as Δt and Δz tend to zero, and a straightforward CFL condition has been chosen. Here, we present a less restrictive CFL condition that allows a greater Δt, thus making simulations faster.

For a given spatial discretization, i.e., a given Δz, the following can be computed before the simulation, where T is the simulation time:

$$M_1 := \max_{j=0,\ldots,N+1} \left\{ \frac{A_{j-1}}{A_{j-1/2}}, \frac{A_j}{A_{j-1/2}} \right\}, \tag{18}$$

$$M_2 := \max_{j=0,\ldots,N+1} \left\{ \frac{A_j + A_{j-1}}{A_{j-1/2}} \right\},$$

$$A_{\min} := \min_{j=0,\ldots,N+1} A_{j-1/2},$$

$$Q_{\max} := \max_{0\le t\le T} Q_{\mathrm{f}}(t),$$

$$\phi_{\max} := \max_{0\le C\le C_{\max}} |f'_{\mathrm{bk}}(C)|,$$

$$d_{\mathrm{comp}}^{\max} := \max_{0\le C\le C_{\max}} d_{\mathrm{comp}}(C), \tag{19}$$

$$d_{\mathrm{disp}}^{\max} := \max_{\substack{-H\le z\le B \\ 0\le t\le T}} d_{\mathrm{disp}}(z, Q(t)).$$

Stable solutions are obtained with (17) if the time step is chosen according to the following CFL condition:

$$\Delta t \le \left(\frac{Q_{\min}}{A_{\min}\Delta z} + \frac{M_1\phi_{\max}}{\Delta z} + \frac{M_2(d_{\mathrm{disp}}^{\max} + d_{\mathrm{comp}}^{\max})}{(\Delta z)^2} \right)^{-1}. \tag{CFL}$$

The proof of this is sketched in the Appendix.

A numerical method for batch sedimentation

In batch sedimentation, we assume that there is no dispersion ($d_{\mathrm{disp}} = 0$) and the boundary condition at both top and bottom is zero flux.

1. Let B denote the distance from the suspension surface to the bottom inside the vessel. Choose the number of layers N, the simulation time T and a large maximum concentration $C_{\max}$.
2. Set $\Delta z := B/N$, compute the concentration $\hat{C}$ at which $f_{\mathrm{bk}}(C)$ has its maximum, the constants M_1, M_2, $\phi_{\max}$ and $d_{\mathrm{comp}}^{\max}$ by (18)–(19). The special case of a constant cross-sectional area gives $M_1 = 1$ and $M_2 = 2$; and a cone implies $M_1 = M_2 = 4$. Choose a time step that satisfies the CFL condition

$$\Delta t \le \left(\frac{M_1\phi_{\max}}{\Delta z} + \frac{M_2\, d_{\mathrm{comp}}^{\max}}{(\Delta z)^2} \right)^{-1}.$$

3. The MOL equations are the following:

$$\begin{aligned}
\frac{\mathrm{d}C_1}{\mathrm{d}t} &= -\frac{A_1 G_1}{A_{1/2}\Delta z} + \frac{A_1\left(D_2^{\mathrm{num}} - D_1^{\mathrm{num}}\right)}{A_{1/2}(\Delta z)^2},\\
\frac{\mathrm{d}C_j}{\mathrm{d}t} &= -\frac{A_j G_j - A_{j-1} G_{j-1}}{A_{j-1/2}\Delta z}\\
&\quad + \frac{A_j\left(D_{j+1}^{\mathrm{num}} - D_j^{\mathrm{num}}\right) - A_{j-1}\left(D_j^{\mathrm{num}} - D_{j-1}^{\mathrm{num}}\right)}{A_{j-1/2}(\Delta z)^2}, \quad j = 2, \ldots, N-1,\\
\frac{\mathrm{d}C_N}{\mathrm{d}t} &= \frac{A_{N-1} G_{N-1}}{A_{N-1/2}\Delta z} - \frac{A_{N-1}\left(D_N^{\mathrm{num}} - D_{N-1}^{\mathrm{num}}\right)}{A_{N-1/2}(\Delta z)^2}.
\end{aligned}$$

Simulations

Constitutive functions. For numerical examples we use the following constitutive functions (Diehl, 2015; Torfs et al., 2017). The hindered settling function is

$$v_{\mathrm{hs}}(C) = \frac{v_0}{1 + (C/\bar{C})^q}, \tag{20}$$

with $v_0 = 0.003\,\mathrm{m/s}$, $\bar{C} = 3.87\,\mathrm{kg/m^3}$ and $q = 3.58$. The effective solids stress function is

$$\sigma_{\mathrm{e}}(C) = \begin{cases} 0 & \text{for } 0 \le C < C_{\mathrm{c}}, \\ \alpha(C - C_{\mathrm{c}}) & \text{for } C \ge C_{\mathrm{c}}, \end{cases} \tag{21}$$

with the critical concentration $C_{\mathrm{c}} = 8\,\mathrm{kg/m^3}$ and $\alpha = 0.5\,\mathrm{m^2/s^2}$. For simulation of an SST, we use the dispersion function by Bürger et al. (2013):

$$d_{\mathrm{disp}}\left(z, Q_{\mathrm{f}}\right) = \begin{cases} \alpha_1 Q_{\mathrm{f}} \exp\left(\dfrac{-z^2/(\alpha_2 Q_{\mathrm{f}})^2}{1 - |z|/(\alpha_2 Q_{\mathrm{f}})}\right) & \text{for } |z| < \alpha_2 Q_{\mathrm{f}}, \\ 0 & \text{for } |z| \ge \alpha_2 Q_{\mathrm{f}}, \end{cases} \tag{22}$$

where $\alpha_1 = 0.001\,\mathrm{m^{-1}}$ and the choice $\alpha_2 = 7.2\,\mathrm{s/m^2}$ implies that $d_{\mathrm{disp}}(z, Q_{\mathrm{f}}) = 0$ outside the SST for the scenarios below.

Simulation of continuous sedimentation. We assume that the volumetric flows vary with time according to

$$\begin{aligned}
Q_{\mathrm{f}}(t) &= \begin{cases} 265\,\mathrm{m^3/h} & \text{if } t \le 55\,\mathrm{h}, \\ 250\,\mathrm{m^3/h} & \text{if } 55\,\mathrm{h} < t \le 170\,\mathrm{h}, \\ 270\,\mathrm{m^3/h} & \text{if } t > 170\,\mathrm{h}, \end{cases}\\
Q_{\mathrm{u}}(t) &= \begin{cases} 65\,\mathrm{m^3/h} & \text{if } t \le 55\,\mathrm{h}, \\ 50\,\mathrm{m^3/h} & \text{if } 55\,\mathrm{h} < t \le 170\,\mathrm{h}, \\ 70\,\mathrm{m^3/h} & \text{if } t > 170\,\mathrm{h}, \end{cases}\\
Q_{\mathrm{e}}(t) &= 200\,\mathrm{m^3/h},
\end{aligned}$$

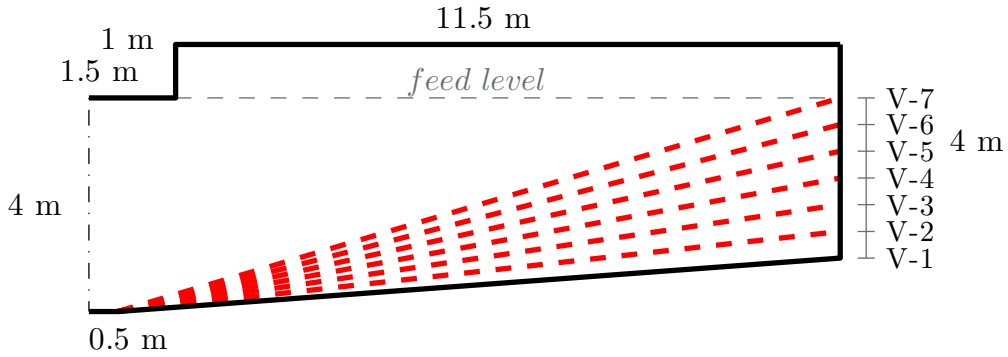

FIGURE 2. Radial profile of half of a rotationally symmetric SST V-1 (black) where the axis of symmetry is the dashed vertical line to the left. The total height is 5 m, $H = 1$ m, $B = 4$ m, the inlet pipe radius is 1.5 m and the outlet radius 0.5 m. The dashed red lines show different slopes of the bottom representing vessels V-2 to V-7.

that the feed concentration is given by

$$C_{\mathrm{f}}(t) = \begin{cases} 5.2\,\mathrm{kg/m^3} & \text{if } t \le 80\,\mathrm{h}, \\ 4.0\,\mathrm{kg/m^3} & \text{if } 80\,\mathrm{h} < t \le 150\,\mathrm{h}, \\ 5.5\,\mathrm{kg/m^3} & \text{if } t > 150\,\mathrm{h}, \end{cases}$$

and that the initial concentration profile is an approximate stationary solution, which is less than the critical concentration down to $z = 1$ m and below increasing towards the bottom:

$$C_0(z) = \begin{cases} 0\,\mathrm{kg/m^3} & \text{if } z < 0\,\mathrm{m}, \\ 0.7\,\mathrm{kg/m^3} & \text{if } 0\,\mathrm{m} \le z \le 1\,\mathrm{m}, \\ \left\{\frac{3}{2}\left(\frac{z}{1\,\mathrm{m}} - 1\right) + 8\right\}\mathrm{kg/m^3} & \text{if } z \ge 1\,\mathrm{m}. \end{cases}$$

For the CFL condition, we set $C_{\max} = 30\,\mathrm{kg/m^3}$ (and check that all simulations stay below this value).

To compare different solutions of the model, we consider the SST studied by Bürger et al. (2012b, Examples 3 and 4), which is vessel V-1 in Figure 2 that has the bottom slope $1.0\,\mathrm{m}/12.5\,\mathrm{m} = 0.08$. The figure also indicates the profiles of further vessels, V-2 to V-7, having the bottom slopes $(0.04, 0.08, 0.12, \ldots, 0.24)$. All vessels have the same cross-sectional area at the top $A(-1\,\mathrm{m}) \approx 523.86\,\mathrm{m^2}$ and bottom $A(4\,\mathrm{m}) \approx 0.78\,\mathrm{m^2}$, and height 5 m but different volumes, from $2300.693\,\mathrm{m^3}$ for V-1 to $1260.405\,\mathrm{m^3}$ for V-7. Due to the inlet pipe, $A(z)$ has a discontinuity at $z = 0$ m.

Simulations were performed during $T = 240$ h (10 days) and the results are shown in Figure 3. Plot (a) for V-1 shows a varying sludge blanket around the depth $z = 1$ m, below which the concentration increases from $C_{\mathrm{c}} = 8\,\mathrm{kg/m^3}$ to above $20\,\mathrm{kg/m^3}$ at the bottom $z = 4$ m. After 170 h the solution approaches a steady state with the concentration below the blanket increasing almost along a straight line towards the bottom. Plots (b) and (c) show that with higher bottom slopes of the vessel, the concentration profiles differ considerably from the case V-1. The higher levels of the sludge blanket shown in Figure 3 (b) and (c) are a natural phenomenon due to the smaller total volumes. The

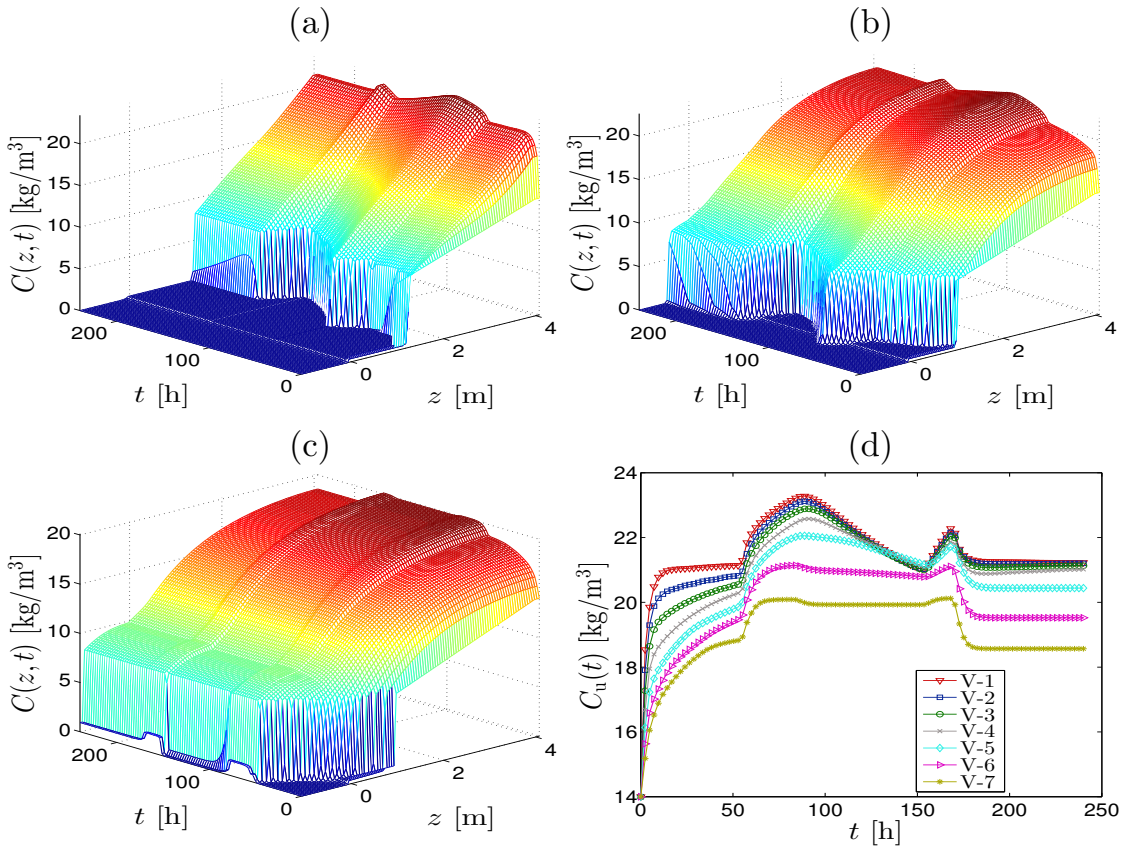

FIGURE 3. (a-c) Simulations results for vessels V-1, V-4 and V-7 and (d) the underflow concentrations $C_u(t)$ of V-1 to V-7.

blanket rises into the clarification zone in V-4 to V-7 due to the decrease in Q_u at $t = 55$ h. At $t = 80$ h there is a reduction in the feed concentration, causing a decrease in the blanket level. After $t = 150$ h the blanket rises again and reaches the effluent level for some of the vessels. The underflow concentrations $C_u(t)$ in plot (d) shows that for times after $t = 50$ h the curves of V-1 to V-3 are close and lie between $C_u = 20.9\,\mathrm{kg/m^3}$ and $23.3\,\mathrm{kg/m^3}$. The maximum value of $23.28\,\mathrm{kg/m^3}$ can be found in V-1. These curves also indicate partly that steady states have almost occurred in the vessels at $T = 240$ h and partly that overflow occurs in V-5 to V-7 in these steady state. This is because the fed mass and the volumetric flows are the same in all vessels and hence a difference in underflow concentrations corresponds to the difference in effluent concentration:

$$Q_u C_u^{\text{V-1}} + Q_e C_e^{\text{V-1}} = Q_f C_f = Q_u C_u^{\text{V-2}} + Q_e C_e^{\text{V-2}}$$
$$\Rightarrow \quad Q_u (C_u^{\text{V-2}} - C_u^{\text{V-1}}) = -Q_e (C_e^{\text{V-2}} - C_e^{\text{V-1}}).$$

Simulations of batch settling. We consider a cone with upper radius 0.3 m and depth $B = 1$ m (the height of the clarification zone $H = 0$ m); see Figure 4 (a). We simulate three scenarios (tests) with different initial concentration profiles $C_0(z)$ during $T = 1$ h. The results are shown in Figure 4 (b)–(d). In simulation (b), the initial concentration is constant $C_0(z) = 4.0\,\mathrm{kg/m^3}$ for $0\,\mathrm{m} \le z \le 1\,\mathrm{m}$, which means that the total mass of solids

is 0.377 kg. The approximate solution C shows that particles settle downwards quickly during the first 13 minutes without concentration discontinuities. After that, the height of sludge blanket varies only slightly, about 1 cm, and the maximum concentration at the bottom increases to 16.24 kg/m^3.

In the next simulation, shown in plot (c), a high concentration is placed on top of pure water. This tests that the numerical method can handle discontinuities decreasing with depth equally well as increasing. We apply the same mass of solids particles as in (b) with initial concentration

$$C_0(z) = \begin{cases} 8.197\,\mathrm{kg/m^3} & \text{if } 0 \le z \le 0.2\,\mathrm{m}, \\ 0\,\mathrm{kg/m^3} & \text{if } 0.3\,\mathrm{m} < z \le 1\,\mathrm{m}. \end{cases}$$

Plot (c) shows that particles settle quickly downwards and start to accumulate at bottom of the vessel from 3 minutes. After a while, the behaviour is similar to test (b).

The last example shown in plot (d) starts with an over-compressed suspension at the bottom:

$$C_0(z) = \begin{cases} 0\,\mathrm{kg/m^3} & \text{if } 0 \le z \le 0.45\,\mathrm{m}, \\ 24.042\,\mathrm{kg/m^3} & \text{if } 0.45\,\mathrm{m} < z \le 1\,\mathrm{m}, \end{cases}$$

and with the mass of particles is the same as before. Plot (d) shows that particles directly start to rise. The bottom concentration increases during 33 minutes to its maximum 28.392 kg/m^3 and then decreases so that the same steady state is reached as in the other cases.

Conclusions

An explicit numerical method for 1D simulation of settling in vessels with varying cross-sectional area has been presented in detail, including the common special case of batch sedimentation in cones, where the vessel area is zero at the bottom. This means that our numerical method can handle the case when there is a singular cross-sectional area, $A(B) = 0$, in the model equation. Previous studies on this problem by Bürger et al. (2004, 2005) have included proof of convergence of the numerical solutions to the exact one of the model PDE. This means that the numerical method is reliable. A novelty in the present work is a new CFL condition, which allows larger time steps and therefore faster simulations. The mathematical proof that the new CFL condition yields reliable simulations is provided in the Appendix.

Simulations of SSTs with the same measurements except for different bottom slopes, hence different total volumes, show how the transient behaviours and concentration profiles differ; however, the underflow concentration is the same in steady state unless an overflow occurs (in agreement with the mass balance). With the simulated scenario, overflow occurs for vessels V-5 to V-7 (see Figure 3 (d)). The benefits of having a steep slope (V-7) for practical reasons should be balanced with drawback of having a higher located sludge blanket with the risk of overflow.

The versatility of the simulation model means that different geometries including the inlet and outlet pipes can be studied to some extent in a 1D model without going to the far more computationally heavy 2D simulation models.

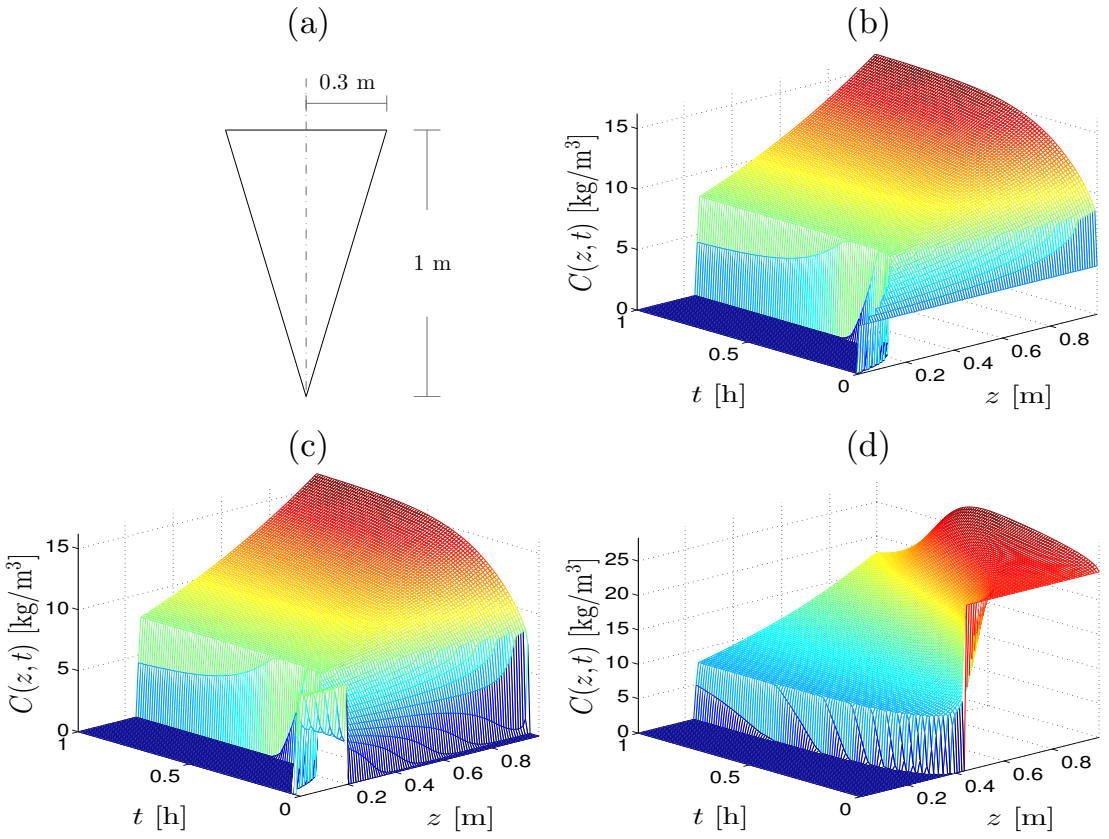

FIGURE 4. (a) Vertical cross-section of cone. (b–d) Simulations of batch tests with different initial concentration distributions.

APPENDIX

CFL estimates. The mathematical purpose of the CFL condition is to ensure that the numerical method is monotone, a property which guarantees that the numerical solution is stable. We refer to Bürger et al. (2005) for definitions and details of standard calculations. Here, we only give the new ingredient. Monotonicity of the update formula (17) means that if C_k^n (for any fixed k) on the right-hand side is perturbed by an increase, then all values C_j^{n+1}, $j = -1, \ldots, N+2$, either remain unchanged or increase. Thus, each new concentration C_j^{n+1} should be an increasing function of all C_k^n at the previous time step; hence, one should check that the following holds for (17):

$$\frac{\partial C_j^{n+1}}{\partial C_k^n} \geq 0 \quad \text{for all } j, k = -1, \ldots, N+2. \tag{A.1}$$

The CFL condition is a means to prove these inequalities. In fact, the CFL is only needed for the cases when $j = k$ in (A.1). The new ingredient here is the numbers A_j and $A_{j-1/2}$ appearing in the numerators and denominators, respectively, of the numerical method; see the right-hand sides of (17). We carry out the proof for a layer in the effluent zone (other

layers are similar or simpler), where the update formula is

$$\begin{aligned} C_j^{n+1} = C_j^n + \Delta t \Bigg[& \frac{Q_{\mathrm{e}}^n}{A_{j-1/2}\Delta z}(C_{j+1}^n - C_j^n) - \frac{A_j G_j^n - A_{j-1} G_{j-1}^n}{A_{j-1/2}\Delta z} \\ & + \frac{1}{A_{j-1/2}(\Delta z)^2}\Big(A_j d_{\mathrm{disp},j}(C_{j+1}^n - C_j^n) - A_{j-1} d_{\mathrm{disp},j-1}(C_j^n - C_{j-1}^n) \\ & + A_j \left(D(C_{j+1}^n) - D(C_j^n) \right) - A_{j-1} \left(D(C_j^n) - D(C_{j-1}^n) \right) \Big) \Bigg]. \end{aligned}$$

We compute

$$\begin{aligned} \frac{\partial C_j^{n+1}}{\partial C_j^n} = 1 - \Delta t \Bigg[& \frac{Q_{\mathrm{e}}^n}{A_{j-1/2}\Delta z} + \frac{\partial}{\partial C_j^n} \left\{ \frac{A_j G_j^n - A_{j-1} G_{j-1}^n}{A_{j-1/2}\Delta z} \right\} \\ & + \frac{A_j d_{\mathrm{disp},j} + A_{j-1} d_{\mathrm{disp},j-1}}{A_{j-1/2}(\Delta z)^2} + \frac{(A_j + A_{j-1})\, d_{\mathrm{comp}}(C_j^n)}{A_{j-1/2}(\Delta z)^2} \Bigg] \end{aligned} \tag{A.2}$$

and estimate the terms in the squared brackets. Clearly, we have

$$\frac{Q_{\mathrm{e}}^n}{A_{j-1/2}\Delta z} \leq \frac{Q_{\max}}{A_{\min}\Delta z},$$

and

$$\frac{A_j d_{\mathrm{disp},j} + A_{j-1} d_{\mathrm{disp},j-1}}{A_{j-1/2}(\Delta z)^2} + \frac{(A_j + A_{j-1})\, d_{\mathrm{comp}}(C_j^n)}{A_{j-1/2}(\Delta z)^2} \leq \frac{M_2(d_{\mathrm{disp}}^{\max} + d_{\mathrm{comp}}^{\max})}{(\Delta z)^2}.$$

For the remaining term, we write out the numerator of the expression within the curled brackets and use the formula (10) to get

$$\begin{aligned} \frac{\partial}{\partial C_j}\left(A_j G_j^n - A_{j-1} G_{j-1}^n \right) &= A_j \frac{\partial}{\partial C_j} \min\left\{ f_{\mathrm{bk}}(\min\{C_j, \hat{C}\}), f_{\mathrm{bk}}(\max\{C_{j+1}, \hat{C}\}) \right\} \\ &\quad - A_{j-1} \frac{\partial}{\partial C_j} \min\left\{ f_{\mathrm{bk}}(\min\{C_{j-1}, \hat{C}\}), f_{\mathrm{bk}}(\max\{C_j, \hat{C}\}) \right\} \\ &= A_j \left\{ \frac{\partial}{\partial C_j} f_{\mathrm{bk}}(\min\{C_j, \hat{C}\}) \text{ or } 0 \right\} - A_{j-1} \left\{ 0 \text{ or } \frac{\partial}{\partial C_j} f_{\mathrm{bk}}(\max\{C_j, \hat{C}\}) \right\} \\ &= \left\{ A_j f_{\mathrm{bk}}'(C_j) \text{ or } -A_{j-1} f_{\mathrm{bk}}'(C_j) \text{ or } 0 \right\}. \end{aligned}$$

Hence,

$$\frac{\partial}{\partial C_j^n} \left\{ \frac{A_j G_j^n - A_{j-1} G_{j-1}^n}{A_{j-1/2}\Delta z} \right\} \leq \frac{M_1 |f_{\mathrm{bk}}'(C_j)|}{\Delta z} \leq \frac{M_1 \phi_{\max}}{\Delta z}$$

and we conclude that (A.2) can be estimated by

$$\frac{\partial C_j^{n+1}}{\partial C_j^n} \geq 1 - \Delta t \left(\frac{Q_{\min}}{A_{\min}\Delta z} + \frac{M_1 \phi_{\max}}{\Delta z} + \frac{M_2(d_{\mathrm{disp}}^{\max} + d_{\mathrm{comp}}^{\max})}{(\Delta z)^2} \right) \geq 0,$$

where the last inequality follows from condition (CFL).

Acknowledgement

RB and JC are supported by BASAL project CMM, Universidad de Chile and Centro de Investigación en Ingeniería Matemática (CI^2MA), Universidad de Concepción. In addition RB is supported by Fondecyt project 1170473; Fondef project ID15I10291, and project CONICYT/FONDAP/15130015.

References

Adimurthi, J. Jaffré, and G. D. Veerappa Gowda. Godunov-type methods for conservation laws with a flux function discontinuous in space. *SIAM J. Num. Anal.*, 42(1):179–208, 2004. doi: http://dx.doi.org/10.1137/S003614290139562X.

R. Bürger, J. J. R. Damasceno, and K. H. Karlsen. A mathematical model for batch and continuous thickening of flocculated suspensions in vessels with varying cross-section. *Int. J. Miner. Process.*, 73:183–208, 2004. doi: http://dx.doi.org/10.1016/S0301-7516(03)00073-5.

R. Bürger, K. H. Karlsen, and J. D. Towers. A model of continuous sedimentation of flocculated suspensions in clarifier-thickener units. *SIAM J. Appl. Math.*, 65:882–940, 2005. doi: 10.1137/04060620X.

R. Bürger, S. Diehl, and I. Nopens. A consistent modelling methodology for secondary settling tanks in wastewater treatment. *Water Res.*, 45(6):2247–2260, 2011. doi: 10.1016/j.watres.2011.01.020.

R. Bürger, S. Diehl, S. Farås, and I. Nopens. On reliable and unreliable numerical methods for the simulation of secondary settling tanks in wastewater treatment. *Computers Chem. Eng.*, 41:93–105, 2012a. doi: 10.2166/wst.2013.239.

R. Bürger, R. Ruiz-Baier, and H. Torres. A stabilized finite volume element formulation for sedimentation-consolidation processes. *SIAM J. Sci. Comput.*, 34:B265–B289, 2012b. doi: 10.1137/110836559.

R. Bürger, S. Diehl, S. Farås, I. Nopens, and E. Torfs. A consistent modelling methodology for secondary settling tanks: A reliable numerical method. *Water Sci. Tech.*, 68(1):192–208, 2013. doi: 10.2166/wst.2013.239.

R. Bürger, J. Careaga, and S. Diehl. Flux identification for scalar conservation laws modelling sedimentation in vessels with varying cross-sectional area. Preprint 2016-40, Centro de Investigación en Ingeniería Matemática, Universidad de Concepción; submitted, 2017.

J. De Clercq, M. Devisscher, I. Boonen, P. A. Vanrolleghem, and J. Defrancq. A new one-dimensional clarifier model – verification using full-scale experimental data. *Water Sci. Tech.*, 47:105–112, 2003. URL `http://wst.iwaponline.com/content/47/12/105`.

S. Diehl. Numerical identification of constitutive functions in scalar nonlinear convection–diffusion equations with application to batch sedimentation. *Appl. Num. Math.*, 95:154–172, 2015. doi: 10.1016/j.apnum.2014.04.002.

S. Diehl, S. Farås, and G. Mauritsson. Fast reliable simulations of secondary settling tanks in wastewater treatment with semi-implicit time discretization. *Computers Math. Appl.*, 70(4):459–477, 2015. doi: 10.1016/j.camwa.2015.05.005.

K. Folens, S. Van Hulle, F. Vanhaecke, and G. Du Laing. Chemical fractionation and speciation modelling for optimization of ion-exchange processes to recover palladium from industrial wastewater. *Water Sci. Tech.*, 73(7):1738–1745, 2016. doi: 10.2166/wst.2016.007.

H. Jiao, A. Wu, H. Wang, S. Zhong, R. Ruan, and S. Yin. The solids concentration distribution in the deep cone thickener: A pilot scale test. *Korean J. Chem. Eng.*, 30 (2):262–268, 2013. doi: 10.1007/s11814-012-0211-0.

J. Park and R. Craggs. Effect of algal recycling rate on the performance of pediastrum boryanum dominated wastewater treatment high rate algal pond. *Water Sci. Tech.*, 70 (8):1299–1306, 2014. doi: 10.2166/wst.2014.369.

R. W. Samstag, J. J. Ducoste, A. Griborio, I. Nopens, D. J. Batstone, J. D. Wicks, S. Saunders, E. A. Wicklein, G. Kenny, and J. Laurent. CFD for wastewater treatment: an overview. *Water Sci. Tech.*, 74(3):549–563, 2016. doi: 10.2166/wst.2016.249.

T. A. Silva, K. A. Freitas, and J. J. R. Damasceno. Experimental evaluation of conical-cylindrical thickeners operanting with aqueous barium sulfate suspensions. *Materials Science Forum*, 416–418:731–736, 2003. doi: 10.4028/www.scientific.net/MSF.416-418.731.

N. Stepova and Yu. I. Kalugin. Mathematical modeling of a secondary clarifier with cone-shaped bottom. *Int. J. Fluid Mech. Res.*, 38(5):458–478, 2011. doi: 10.1615/InterJFluidMechRes.v38.i5.70.

E. Torfs, T. Maere, R. Bürger, S. Diehl, and I. Nopens. Impact on sludge inventory and control strategies using the benchmark simulation model no. 1 with the Bürger-Diehl settler model. *Water Sci. Tech.*, 71(10):1524–1535, 2015. doi: 10.2166/wst.2015.122.

E. Torfs, S. Balemans, F. Locatelli, S. Diehl, R. Bürger, J. Laurent, P. Françis, and I. Nopens. On constitutive functions for hindered settling velocity in 1-d settler models: Selection of appropriate model structure. *Water Res.*, 110:38–47, 2017. doi: 10.1016/j.watres.2016.11.067.

P. van der Steen, K. Rahsilawati, A. Rada-Ariza, C. Lopez-Vazquez, and P. Lens. A new photo-activated sludge system for nitrification by an algal-bacterial consortium in a photo-bioreactor with biomass recycle. *Water Sci. Tech.*, 72(3):443–450, 2015. doi: 10.2166/wst.2015.205.

R. W. Watts, S. A. Svoronos, and B. Koopman. One-dimensional clarifer model with sludge blanket heights. *J. Environ. Eng.*, 122(12):1094–1100, 1996.

D. A. White and N. Verdone. Numerical modelling of sedimentation processes. *Chem. Eng. Sci.*, 55:2213–2222, 2000. doi: 10.1016/S0009-2509(99)00496-0.